Direct Meso-Scale Simulations of Fibres in Turbulent Liquid Flow

J. J. Derksen*

Chemical & Materials Engineering Department, University of Alberta, Edmonton, AB, Canada T6G 2G6, Canada

A procedure for direct, meso-scale simulations of flexible fibres immersed in liquid flow is introduced. The fibres are composed of chains of spherical particles connected through ball joints with the bending stiffness of the joints as a variable. The motion of the fibres and the liquid is two-way coupled with full resolution of the solid–liquid interface. First the simulation procedure is validated by means of an analytical solution for sphere doublets in zero-Reynolds simple shear flow. Subsequently we use the numerical method to study inertial flows with fibres, more specifically the interaction of a fibre with isotropic turbulence.

Une procédure pour des simulations directes à la méso-échelle de fibres souples immergées dans la circulation de liquide est présentée. Les fibres sont composées de chaînes de particules sphériques reliées par des joints à rotule avec la rigidité à la flexion des joints comme variable. Le mouvement des fibres et du liquide est bidirectionnel avec une résolution intégrale de l'interface solide-liquide. D'abord, la procédure de simulation est validée au moyen d'une solution analytique pour les doublets de sphère dans un écoulement de cisaillement simple à nombre de Reynolds nul. Par la suite, nous utilisons la méthode numérique pour étudier les flux inertiels avec les fibres, plus précisément l'interaction d'une fibre avec la turbulence isotrope.

Keywords: liquid–solid flow, mesoscopic, lattice-Boltzmann, direct simulations, fibres

INTRODUCTION

Motivated by applications in pulp handling, flow of polymer solutions, and crystallisation processes (to mention a few examples only) we study the mutual interaction between fibres, and interactions of fibres with liquid flow, specifically turbulent liquid flow. The details of these interactions matter for characterising the rheological behaviour of fibre suspensions, for understanding conditions for fibre coagulation (Schmid and Klingenberg, 2000), and for assessing breakage probability of crystalline needles (stiff fibres) or flexible fibres as a result of fluid deformation. For this we are building direct numerical simulation tools, with an emphasis on a computational procedure that allows for the incorporation of inertial effects (of liquid and fibres) so that also non-colloidal and/or turbulent systems can be studied.

In this paper the modeling approach will be outlined, a basic validation presented, and the simulated behaviour of a fibre in a turbulent field discussed. The simulation procedure zooms in on the mesoscopic level, that is, the direct computation of the motion of a limited number (a few hundred max) of fibres fully coupled to the liquid flow, with resolution of the solid–liquid interfaces. The goal of the simulations is to capture the essential physics at the scale of a collection of fibres, for a better understanding and modeling of fibre suspensions at the macro (e.g., process) scale.

In our computational approach fibres consist of spherical particles connected through ball joints (similar to Qi, 2007) that have specified bending stiffness. The liquid flow solver is based on the lattice-Boltzmann scheme, with an immersed boundary method that resolves the no-slip condition at the spheres' surfaces. The immersed boundary method provides the hydrodynamic forces and torques on the spheres that we use for integrating their linear and rotational motion. The spheres' motion is constrained by the joints. These constraining conditions are employed to determine the forces and torques required to maintain the integrity of the fibres. Comparing the joint-related forces and torques with fibre strength allows us to assess fibre breakage probabilities. The

*Author to whom correspondence may be addressed.
E-mail address: jos@ualberta.ca
Can. J. Chem. Eng. 88:677–681, 2010

DOI 10.1002/cjce.20303
Published online 5 May 2010 in Wiley InterScience
(www.interscience.wiley.com)

spheres (within the same or within different fibres) undergo elastic collisions by means of a soft-sphere scheme. Also, when two or more spheres get in close proximity (mutual distance smaller than the grid spacing) we explicitly determine radial lubrication forces to capture that part of their hydrodynamic interactions that is not resolved by the finite resolution of the lattice-Boltzmann scheme.

SIMULATION SETUP AND SETTINGS

Liquid Flow and Solid–Liquid Coupling

For solid–liquid suspensions we have a direct simulation procedure in place to solve for the liquid flow based on the lattice-Boltzmann method (LBM) (Succi, 2001), and that couples the liquid flow and the motion of solid spheres suspended in it. For the latter: at the surface of each sphere the fluid velocity is forced to match the local velocity of the solid surface (which is the sum of the linear velocity $\mathbf{V}_p$, and rotation $\Omega_p \times (r - r_p)$ with Ω_p the angular velocity of the sphere, $\mathbf{r}_p$ the centre position of the sphere, and $\mathbf{r}$ a point on its surface). The details of this forcing scheme can be found elsewhere (Derksen and Van den Akker, 1999). The collections of forces representing the no-slip condition at the spheres' surfaces are added up to determine the hydrodynamic force and torque acting on each sphere (action = −reaction). These are used to evaluate the equations of linear and rotational motion of the spheres. The spatial resolution of the simulations is such that the particle radius a spans six lattice spacings. Grid sensitivity studies and favourable experimental validation (in terms of single particle motion and the flow field surrounding it) demonstrate that this is sufficient resolution (Ten Cate et al., 2002) for moderate Reynolds numbers (up to 15, based on slip velocity and a).

For multiple particle simulations additional features relate to particle–particle interactions. Hydrodynamic interaction between the spheres is taken care of by the LBM as long as the sphere surfaces are not too close. If they are within one lattice spacing (i.e., roughly $0.15a$) the LBM is not able to accurately represent the hydrodynamic interaction between the spheres anymore (Nguyen and Ladd, 2002). In such situations the analytical solution for the radial lubrication force is explicitly invoked. This force diverges for $h \to 0$as$1/h$ with h the distance between sphere surfaces. With a view to numerical stability, and also physical concepts such as surface roughness, and the continuum assumption we saturate the lubrication force at very close proximity (at $2.0 \times 10^{-4}a$ in the current simulations) of two spheres.

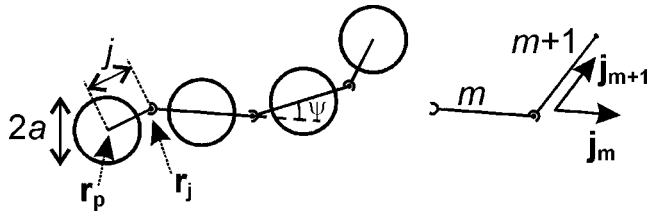

Figure 1. Definition of fibres as spheres connected through joints. Right: definition of the rod vectors $\mathbf{j}_m$.

For direct sphere–sphere collisions a soft-sphere approach has been implemented. Given the constraints on particle motion as a result of the joints, a soft-sphere approach is to be preferred over hard-spheres. If particle surfaces are within a certain distance ($3.0 \times 10^{-3}a$ in the current simulations) a linear elastic repulsive force is switched on. This effectively prevents the particles from overlapping. By performing granular simulations with the soft-sphere scheme we checked and succeeded in conserving energy making the sphere–sphere collisions fully elastic.

Definition of Fibres

The fibres are defined as solid spheres connected through rods and ball joints, see Figure 1. The rods and joints have no mass so that the fibre mass is concentrated in the solid spheres. The parameters defining a fibre are the radius of the spheres it is made of (a), the density of the solid material (relative to the liquid density), the length of the rods j that connect the spheres with the joints, the number of spheres per fibre N, and the properties of the ball joints. In this paper three types of joints will be considered: (1) completely stiff joints, not allowing for an angle (ψ, see Figure 1) unequal zero between the rods; (2) fully flexible joints, that is, joints that cannot exert a torque; (3) joints with a finite bending stiffness, and zero torsion stiffness. In the latter case the bending torque is proportional to the vector product of the vectors defining the two rods connected by the joint (see the right panel of Figure 1):

$$\mathbf{T}_{jm} = -\gamma \frac{\mathbf{j}_m \times \mathbf{j}_{m+1}}{j^2} \tag{1}$$

with γ the stiffness parameter. In terms of the bending stiffness (EI, elastic modulus × area moment of inertia) of a beam: $EI \propto \gamma j$.

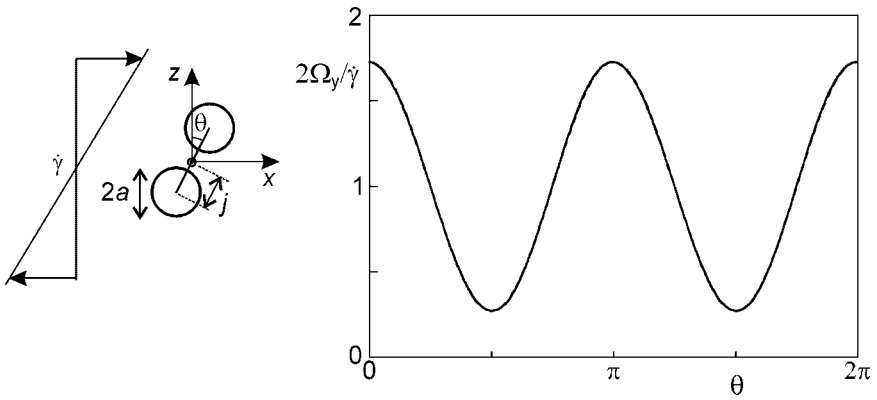

Figure 2. Left: Definition of the shear-flow validation case. Right: Rotation rate of the sphere doublet as a function of the angle θ for $j/a = 1.5$. Closely spaced symbols: simulation; drawn line: least squares fit (line and symbols are hard to distinguish).

Table 1. Angular velocity coefficient C (Equation 2) as a function of the ratio j/a

j/a	C (simulation)	C (analytical)
1.2	0.659	0.654
1.5	0.728	0.724
2.0	0.807	0.805

Analytical results due to Arp and Mason (1977).

The forces at the joints are determined such that the fibre keeps its integrity. This means that if we update the linear and angular velocity of a particle m and a particle $m+1$ in the fibre, the joint connecting them must have a unique velocity (i.e., must have the same velocity from the perspective of particle m and particle $m+1$). For a fibre having N particles, and thus $N-1$ joints, the integrity condition leads to a linear system of $3(N-1)$ equations in the $(N-1)$ three-dimensional force vectors at the joints $F_{jm}, m=1\ldots(N-1)$. This linear system we solve for each fibre, each time step. The forces and torques acting on each sphere (hydrodynamic due to the LBM, lubrication, soft-sphere-related, and joint-related) are added up in order to integrate the spheres' linear and rotational equations of motion.

Fibre-in-Turbulence Simulations Setup

For studying the interaction between fibres and turbulence, we place a single fibre in a three-dimensional, cubic, fully periodic

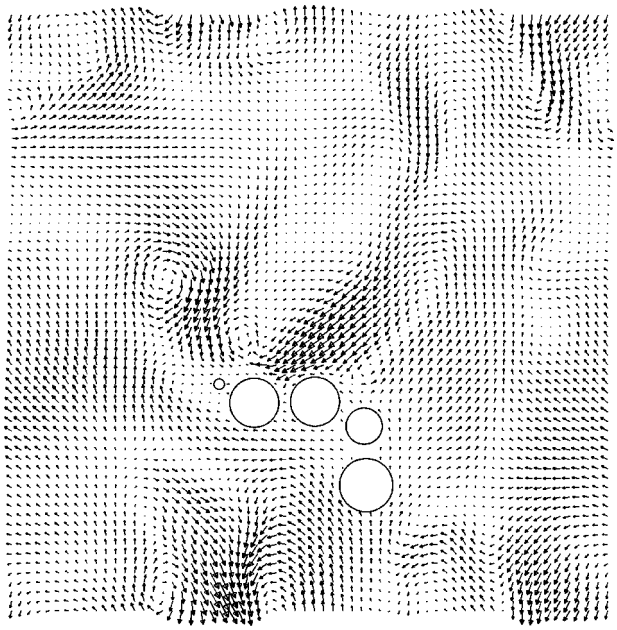

Figure 3. Cross-section in terms of velocity vectors through the 128^3 fully periodic domain. The circles are the cross-sections of the spheres. The resolution is such that one in four vectors is on display.

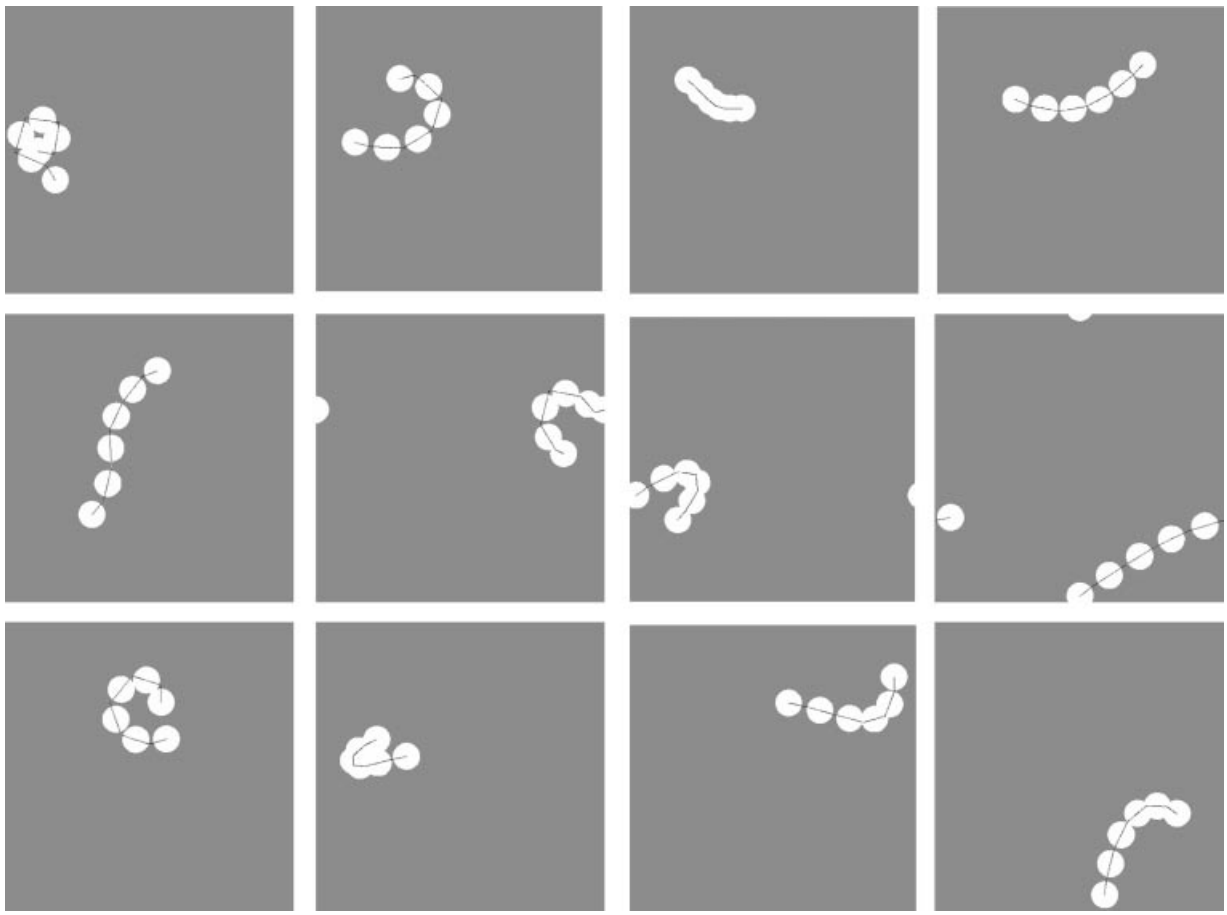

Figure 4. Side views of fibres in the 128^3 periodic domain, three snapshots per case. From left to right: increasing bending stiffness γ (Equation 1): $\gamma/(12\pi\nu\rho a^2 u_{\mathrm{rms}}) = 0$, 1.78, 14.2, 56.8.

domain. The default domain size is 128^3 lattice nodes. (For comparison: the spheres forming the fibre have a diameter $2a = 12$ lattice spacings). In the computational domain we create a homogeneous, isotropic turbulent flow by linear forcing (Rosales and Meneveau, 2005). In the linear forcing method turbulence is sustained by a force on the fluid that is proportional to the local velocity. The fluid develops isotropic and (due to the full periodicity of the three-dimensional domain) homogeneous turbulence with Kolmogorov spectral characteristics (see Rosales and Meneveau, 2005). This flow is characterised by its time and space averaged energy dissipation rate $\bar{\varepsilon}$ and the root-mean-square velocity u_{rms} of the liquid. From these quantities measures for the Kolmogorov scales and relevant Reynolds numbers are derived. The single fibre released in this domain has a solid over fluid density ratio $\rho_{\mathrm{s}}/\rho_{\mathrm{f}} = 3.0$, and consists of six spheres. Our main interest is in how fibres with different stiffness respond to turbulence.

We are particularly interested in cases with strongly inhomogeneous flows around the spheres constituting the fibres so that they are subjected to erratic hydrodynamic forces that twist and bend them. The level of inhomogeneity of flow around the spheres is expressed as the ratio of sphere radius and Kolmogorov length scale: $a/\eta_{\mathrm{K}} = a(\nu^3/\bar{\varepsilon})^{-1/4}$ that has been set to 8.1. The Reynolds number associated with the flow around the spheres is: $Re_{\mathrm{rms}} = (u_{\mathrm{rms}}a)/\nu = 25$.

VALIDATION: SPHERE DOUBLETS IN SIMPLE SHEAR

Before discussing the turbulence simulations we report on a numerical experiment intended to validate (at least partly) our numerical procedure. The case considered is a (degenerate) fibre consisting of two spheres, stiffly linked together in simple shear flow at low Reynolds number ($\mathrm{Re} = \dot{\gamma}a^2/\nu$); see Figure 2, left panel. In simple shear the fibre rotates around the y-axis with an angular velocity that depends on its orientation:

$$\Omega_{\mathrm{y}} \equiv \frac{\mathrm{d}\theta}{\mathrm{d}t} = \frac{1}{2}\dot{\gamma}(1 + C\,\cos(2\theta)) \tag{2}$$

The parameter C is a function of the spacing between the spheres (Arp and Mason, 1977). The special case with $j = a$ (two touching spheres) has been discussed in a previous paper (Derksen, 2008). In Figure 2 (right panel) we show simulation results in terms of Ω_{y} as a function of θ if $j = 1.5a$. The least-squares fit in that figure has $C = 0.728$; the analytical result for this case is $C = 0.724$ (Arp and Mason, 1977). In Table 1 we summarise more cases, showing good agreement of the numerical with the analytical solutions.

FIBRES IN TURBULENCE

Now that we have established some confidence in our way to simulate fibres in liquid flow, we turn to fibres immersed in turbulent flow. A typical realisation of the flow in a cross-section through the 128^3 domain is given in Figure 3. The circles represent the spheres constituting the fibre. The six spheres constituting the fibre have the same size. However, not all spheres are visible in the cross-section; and not all spheres visible are cut in the same manner. The figure illustrates the size of the turbulent structures relative the sphere diameter. In Figure 4 we show single realisations of fibres with different bending stiffness γ (Equation 1), released in turbulent flows with constant statistical properties. Obviously turbulence has a harder job bending the stiffer fibres. To make this a more objective and quantitative statement we plot time series of the fibre-averaged angle $\bar{\psi}$ (the average absolute angle of the five joints in the fibre) in Figure 5. The maximum angle $\psi_{\max}$ is reached when the fibre is bent such that two neighbouring spheres touch: $\cos(1/2\psi_{\max}) = a/j$. The fibre-averaged angle strongly fluctuates in time. For the fully flexible fibre ($\gamma = 0$) the state of maximum bending $\bar{\psi} = \psi_{\max}$ is approached regularly. With increased stiffness the fibre-averaged angle decreases.

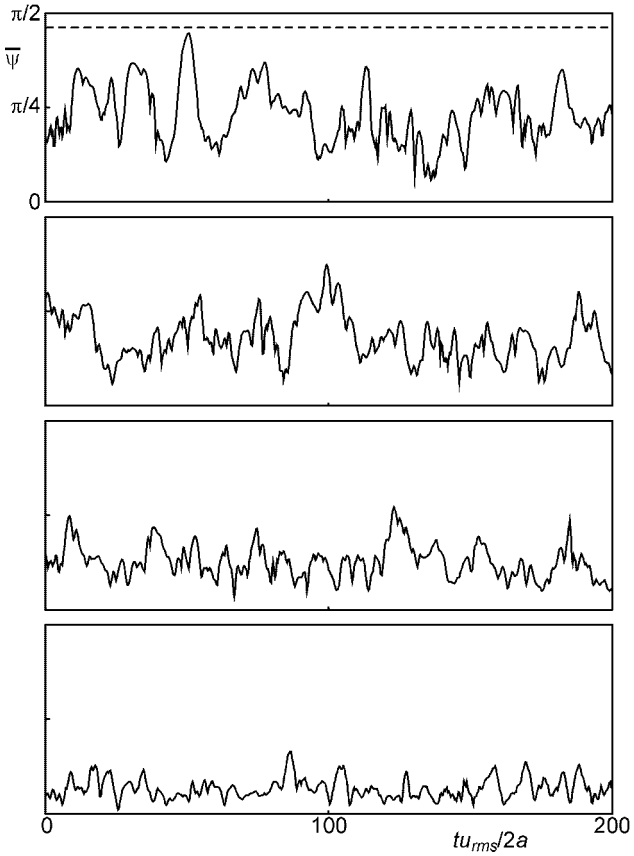

Figure 5. Time series of the fibre-averaged angle $\bar{\psi}$ with from top to bottom increasing bending stiffness $\gamma/(12\pi\nu\rho a^2 u_{\mathrm{rms}}) = 0$, 1.780, 14.2, 56.8. The dashed line in the upper panel represents $\psi_{\max}$ (see text).

In Figure 6 we have summarised the main results so far. It shows the decay of the time-averaged, fibre-averaged angle with increasing bending stiffness. The bending stiffness has been non-dimensionalised with the torque related to the Stokes drag force at slip velocity u_{rms} times the particle diameter $2a$. In Figure 6 we also plot the time-averaged forces and torques in the joints. The symbols F_{j} and T_{j} denote the time-averaged, fibre-averaged absolute values; for example, $T_{\mathrm{j}} = \left\langle 1/5 \sum_{m=1}^{5} \left| T_{jm} \right| \right\rangle$ for a fibre with six spheres (and five joints), $\langle\,\rangle$ denotes time averaging. The force is quite insensitive of the fibre stiffness; it is roughly five times the Stokes drag on a sphere with slip velocity u_{rms}. Since the flow around the fibre is very inhomogeneous, apparently the details of the fibre morphology (level of stretching) do not matter much for the forces at the joints. Obviously the torque is dependent on the fibre stiffness with the torque being zero at $\gamma = 0$ by definition.

SUMMARY

In this preliminary study we introduced a direct method for simulating the interactions of fibres and (turbulent) fluid flow. Fibres

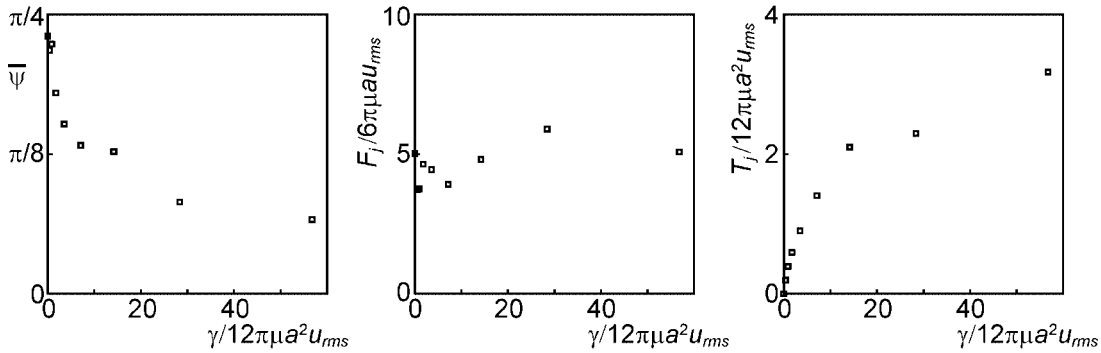

Figure 6. Time-averaged, fibre-averaged angle, absolute joint force, and absolute joint torque (from left to right) as a function of the fibres' bending stiffness γ.

were built of spherical particles connected through joints. We validated the method with an analytical solution for dumbbells in simple shear flow under creeping flow conditions. Subsequently we studied the behaviour of a single fibre released in homogeneous, isotropic turbulence (with the Kolmogorov scale typically smaller than the sphere size) with a focus on the response of the fibre as a function of its stiffness. The stiffness has a marked effect on the level of bending (and stretching) of the fibre. The forces needed to hold the fibre in tact were quite independent of the bending stiffness.

In future work we will broaden the parameter space with turbulence properties (more specifically fibre and sphere size relative to the Kolmogorov length scale), and on fibre-fibre interactions in vigorous turbulent flow. With respect to the latter: for fibre clustering (as experimentally observed in many studies) it is considered essential for the direct contact between fibres to have stickiness, or friction and non-ideal collisions (Schmid and Klingenberg, 2000). In direct simulations on fibre–fibre interactions we would be able to investigate the detailed nature of such direct contact required for fibres to cluster and to distinguish between the effects of direct contact and of the interstitial liquid. Also the role of a fibre size distribution on the collective behaviour of a fibre suspension could be investigated.

NOMENCLATURE

a	radius of sphere
C	parameter in Equation (2)
$\mathbf{F}_{jm}$	force in joint m
F_j	fibre and time averaged absolute force
h	distance between sphere surfaces
$\mathbf{j}_m$	rod vector
j	length of rod
N	number of spheres per fibre
$\mathbf{r}$	position vector
$\mathbf{r}_p$	centre position of sphere
$\mathbf{T}_{jm}$	torque in joint m
T_j	fibre and time averaged absolute torque
u_{rms}	root-mean-square velocity
$\mathbf{v}_p$	(linear) velocity of sphere
γ	fibre stiffness
$\dot{\gamma}$	shear rate
$\varepsilon, \bar{\varepsilon}$	(average) dissipation rate
η_K	Kolmogorov length scale
θ	doublet orientation
ν	kinematic viscosity
ρ_s, ρ_f	solid and liquid density
$\psi, \bar{\psi}, \psi_{max}$	angle between rods (and fibre-averaged, and maximum angle)
Ω_p	angular velocity of sphere
Ω_y	doublet's angular velocity
Re, Re_{rms}	Reynolds number (based on rms velocity)

REFERENCES

Arp, P. A. and S. G. Mason, "The Kinetics of Flowing Dispersions," J. Coll. Interface Sci. **61**, 21–43 (1977).

Derksen, J. J., "Flow-Induced Forces in Sphere Doublets," J. Fluid Mech. **608**, 337–356 (2008).

Derksen, J. and H. E. A. Van den Akker, "Large-Eddy Simulations on the Flow Driven by a Rushton Turbine," AIChE J. **45**, 209–221 (1999).

Nguyen, N.-Q. and A. J. C. Ladd, "Lubrication Corrections for Lattice-Boltzmann Simulations of Particle Suspensions," Phys. Rev. E. **66**, 046708 (2002).

Qi, D., "A New Method for Direct Simulations of Flexible Filament Suspensions in Non-Zero Reynolds Number Flows," Int. J. Numer. Meth. Fluids **54**, 103–118 (2007).

Rosales, C. and C. Meneveau, "Linear Forcing in Numerical Simulations of Isotropic Turbulence: Physical Space Implementations and Convergence Properties," Phys. Fluids **17**, 095106 (2005).

Schmid, C. F. and D. J. Klingenberg, "Mechanical Flocculation in Flowing Fiber Suspensions," Phys. Rev. Lett. **84**, 290–293 (2000).

Succi, S., "The Lattice Boltzmann Equation for Fluid Dynamics and Beyond," Clarondon Press, Oxford (2001).

Ten Cate, A., C. H. Nieuwstad, J. J. Derksen and H. E. A. Van den Akker, "PIV Experiments and Lattice-Boltzmann Simulations on a Single Sphere Settling Under Gravity," Phys. Fluids **14**, 4012–4025 (2002).

Manuscript received November 19, 2009; revised manuscript received January 20, 2010; accepted for publication January 26, 2010